Combustion and Flame 228 (2021) 250–258

Contents lists available at ScienceDirect

Combustion and Flame

journal homepage: www.elsevier.com/locate/combustflame

In-operando thermophysical properties and kinetics measurements of Al-Zr-C composites

Dylan J. Kline[a,b], Miles C. Rehwoldt[a,b], Jeffery B. DeLisio[c], Sara C. Barron[c], Haiyang Wang[a], Zaira Alibay[a], Juan C. Rodriguez[c], Gregory M. Fritz[c], Michael R. Zachariah[a,*]

[a] University of California Riverside, Riverside, CA 92521, USA
[b] University of Maryland College Park, College Park, MD 20742, USA
[c] The Charles Stark Draper Laboratory, Inc., Cambridge, MA 02139, USA

ARTICLE INFO

Article history:
Received 14 October 2020
Revised 26 December 2020
Accepted 29 December 2020

Keywords:
Energetic materials
Synthesis
Thermophysical properties
Reaction kinetics
Temperature measurements

ABSTRACT

This work investigates the combustion velocity, thermophysical properties, and reaction activation energies of Al-Zr-C nanolayered composite microparticles undergoing gasless high-temperature propagation after preparation via additive manufacturing. High-speed videography and pyrometry of the reaction event were used to analyze two Al-Zr-C samples with varied stoichiometry. Combustion velocity of the Al-Zr-C composites was ~0.3–0.5 cm/s and varied inversely with the Al content in the system. The Al-Zr-C composites also exhibited auto-oscillations during the propagation event which were characterized to have temperature fluctuations of ~50–100 K with a periodicity of ~1 Hz. Temperature data collected via color ratio pyrometry was used to measure the thermal profile in-operando. Temperature maps were used to estimate the thermal diffusivity of the samples to be ~2 × 10^{-6} m^2/s on the leading edge of the reaction front with a >30x increase in thermal diffusivity on the trailing edge. The activation energy for the Al-Zr-C composites was estimated to be ~30–35 kJ/mol under reacting conditions. This work ultimately demonstrates an accessible measurement methodology that could be used to estimate thermophysical changes in materials for generalized modeling purposes and confirms the functionality of the materials to create conductive pathways after reaction.

1. Introduction

Energetic materials from the perspective of high-temperature synthesis systems have experienced a revived research interest with the rise of new manufacturing methods [1–4] and new experimental characterization techniques (high-speed videography/microscopy) [5–7]. Many efforts in the literature have investigated structure-function relationships by studying changes in the chemical formulation [5,8,9] or by changing the physical architecture of the samples using different manufacturing methods [2,10], material properties [11–13], or additives that may alter propagation rates [14–17]. These studies have, for the most part, focused on the behavior of thermite systems (metal fuel/metal oxide oxidizer), which are a subset of self-propagating high-temperature synthesis (SHS) systems [18]. Comparison studies on these materials have attempted to independently modify thermochemical and architectural parameters, though they are inherently entangled. For example, changes in stoichiometry may change chemistry and also change overall thermophysical properties [14,15]. The multiphase nature of energetic material reactions only further complicates the process of making reliable thermophysical measurements.

In contrast to many energetic reactions where fast pressurization and energy release occurs, the SHS process can be “gasless,” achieve similar temperatures, and nearly all final products are condensed phase since the process is typically an exothermic metal alloying process [19]. SHS has been widely studied since the early 1970s as a method to produce powders or ceramics. Materials for SHS are generally mixtures of micron-sized metal powders that have been mechanically milled into composite materials that will react and propagate at ~1 cm/s [19–21]. Significant strides have been made by others to develop models for the heat transfer and kinetics of these reactions [20,22,23]. Although some SHS composites prepared by arrested reactive milling release gas, for this study, the condensed phase nature of intermetallic SHS reactions are favorable for a diagnostic case study [24,25].

A fundamental aspect of heterogenous, solid, self-sustained interface driven reactions is the interplay between the heat flux to initiate the reaction and the heat generated from reaction. At a macroscopic level, nearly all SHS systems act in a “quasi-

* Corresponding author.
E-mail addresses: mrz@engr.ucr.edu, mrz@umd.edu (M.R. Zachariah).

https://doi.org/10.1016/j.combustflame.2020.12.045
0010-2180/

homogenous" manner whereby the reaction front of the SHS system moves uniformly in the direction of propagation [18,26]. This can simply described by saying that the heat flux smoothly delivers heat forward for initiation to nearby unreacted materials [18,27,28]. Steady-state, quasi-homogenous SHS systems may be quantified analytically by Eq. (1) where v is propagation velocity, α is effective thermal diffusivity, $\dot{\omega}$ is reaction rate, T_{ad} is adiabatic flame temperature, T_i is ignition temperature, and T_0 is the temperature of the unreacted material [28]. Eq. (1) simply suggests that the propagation rate is dependent on how much energy is released (T_{ad}), how fast the energy is released ($\dot{\omega}$), and how fast that energy can be transported to nearby unreacted reactions (α).

$$v \approx \sqrt{\alpha \cdot \dot{\omega}\left(\frac{T_{ad}-T_i}{T_i-T_0}\right)} \tag{1}$$

This study will focus on the self-propagating, high-temperature synthesis of Al-Zr-C nanolayer composites prepared by arrested reactive ball milling and subsequently 3D printed. This mixture has particular applications as a composite that can be reacted to form electrically conductive paths as detailed in concurrently-prepared articles by Arlington et al. [29,30] and previously patented by Fritz and Barron [31]. Al-Zr-C composites have been largely studied prior to this for ZrC particle synthesis, but much of the research has only been reported by one group and reiterated numerous times [21,32–34]. Previous work reports that the reaction is initiated by Al melting (~933 K) followed by an exothermic alloying process with Zr to form Zr_xAl_y (Eq. (2)) [21,32–35]. The C then dissolves into the mixture to form a slurry of $Zr_xAl_yC_m$ (Eq. (3)) until a saturation point where ZrC particles begin nucleating (Eq. (4)). The final products of the SHS reaction are mixtures of Al, Zr, and Zr_xAl_y alloys with small ZrC particles interspersed throughout. It has also been shown that some AlC_m can be found in the final products (Eq. (5)) [21,32–34]. The ideal overall reaction for the Al-Zr-C system is shown in Eq. (6) as the ZrC formation reaction, in which $\Delta H_{rxn} = -196.6$ kJ/mol.

$$Zr\ (s) + Al\ (l) \rightarrow Zr_xAl_y\ (l) + Zr\ (s,l) + Al\ (l) \tag{2}$$

$$Zr_xAl_y\ (l) + C\ (s) \rightarrow Zr_xAl_yC_m\ (l) \tag{3}$$

$$Zr_xAl_y\ (l) + C\ (s) \rightarrow ZrC\ (s) + Al\ (l) \tag{4}$$

$$Al\ (l) + C\ (s) \rightarrow AlC_m\ (l) \tag{5}$$

$$Al\ (l) + C\ (s) \rightarrow AlC_m\ (l) \tag{6}$$

Research on SHS materials has largely relied on measurements taken with highly specialized diagnostics like time-resolved X-ray diffraction (TRXRD), high-speed transmission electron microscopy (HSTEM), or dynamic transmission electron microscopy (DTEM), though these tools can be prohibitively expensive and time intensive despite offering *in-operando* observations [20]. These *in-operando* devices also typically involve experiments that are performed under nonstandard conditions (e.g., in vacuum), on small amounts of material, and generally do not offer simultaneous temperature measurements for thermophysical property and kinetics estimations. However, others have found success measuring the thermophysical properties and kinetic parameters of SHS reactions using temperature measurements which has served as the inspiration for the work here [20,36,37]. This study observes and quantifies flame front behavior through an *in-operando* probe of the thermophysical and kinetic properties of an Al-Zr-C SHS material using high-speed color camera pyrometer. Thermochemical parameters can be used as inputs for a simple thermal reaction propagation models for predictive modeling of propagation rates in SHS materials based on easily measured input parameters. Additionally, the in-operando spatiotemporal temperature measurements of the SHS reaction will be used to gain insight on the reaction mechanism in the material.

Table 1
Mixture compositions for the two samples tested in this study. Number in sample description denotes atom ratio of reactants in composite.

Sample	Mass%		
	Al	Zr	C
2 Al / 1.2 Zr / 1 C	31%	62%	7%
0.5 Al / 1.2 Zr / 1 C	10%	81%	9%

2. Methods

2.1. Sample preparation

The powder samples were prepared by Charles Stark Draper Laboratory (CSDL) (Cambridge, MA, USA) and Johns Hopkins University (Baltimore, MD, USA) as part of the RAIL3D program and previously patented as "Reactively assisted ink for printed electronic circuits" [31]. A full characterization of these powders is described in concurrently prepared articles by Arlington et al. [29,30] In summary, these powders were prepared by arrested reactive ball milling. The mass loading of the powders was chosen to give an Al:Zr:C atomic ratio of 2:1.2:1 or 0.5:1.2:1. After milling, powders were dried in air and sieved to less than 25 micrometers. The composition of the two tested samples can be seen in Table 1.

Samples used in this study were prepared by direct-write additive manufacturing (3D printing) of an ink containing one of two different stoichiometries as described in Arlington et al. [29,30] Prior to printing, the precursor was loaded into a 10 mL plastic syringe with a tapered 18-gage blunt Luer Lock needle (McMaster-Carr) and placed into a vertically mounted syringe pump on the 3D printer (Hyrel3D). The syringe pump extrudes material along an 8-cm square perimeter path that has 12 microscope coverslips (22 × 22 mm, 0.17 mm thickness, VWR) placed along the path. Four layers of material was printed for each batch of 12 samples for a final approximate height of ~2.5–3 mm. Samples were then placed on a hot plate at ~100C for ~10 min to evaporate any remaining dimethylformamide (DMF) from the samples and are then broken apart using a razor. Samples were printed to this height to minimize the effect of thermal loss through interactions with the glass substrate on which they were mounted that could possibly skew values for temperature and propagation rate.

2.2. Morphology characterization

Reactive powders and printed samples were analyzed with scanning electron microscopy (SEM) using a Duobeam Quanta 200i (see Fig. S1). SEM analysis of the Al-Zr-C system focuses on the particle separation distance, particle sizes, and particle morphology. From Fig. S1, one can see that reactant particles within both systems considered are mostly non-spherical with length scales <10–20 μm as a result of the sieving process. Separation distances appeared to be no larger than a couple microns, which seems reasonable given that the mode of additive manufacturing relies on the evaporation of a solvent, and the resulting materials are expected to be quite porous.

2.3. High-speed videography/pyrometry

Macroscale burn tests were performed by mounting the microscope coverslips with printed SHS material on a 3-axis trans-

lational stage (Newport) inside of a container filled with argon and observing the combustion event using high-speed videography. Samples were ignited using a resistively heated nichrome wire and the reaction event was recorded using a high-speed color camera (Phantom VEO710) recording at ~200 frames/s. The camera was equipped with a macro lens that allows for a spatial resolution of ~20 μm/pixel (Nikon). The propagation velocity for each sample was estimated by tracking the location of the reaction front throughout the video and using the pixel/distance ratio to calculate distance traveled over time. Samples were tested three times each and propagation rate was averaged over each of the videos using a linear best fit. A separate experiment to observe the homogeneity of the reaction front used the same high-speed camera equipped with a long working distance microscope objective which gives a spatial resolution of ~1.7 μm/pixel (InfinityOptics K2 DistaMax).

The high-speed color camera was also calibrated to operate as a pyrometer enabling both temporal and spatial temperature measurement of the reacting samples. This capability has been described in detail in previous work [5]. Briefly, raw pixel values were extracted from raw images and demosaiced in accordance with the camera's Bayer filter array to recover red, green, and blue color intensities at every pixel [5]. The color channel ratios were then calculated and corrected using calibration factors obtained for the camera using a blackbody radiation source [5]. Corrected color ratios were then matched to a temperature assuming gray body emission. The final temperatures reported in the 2D temperature map are below the saturation threshold, above the black level of the camera, and are accurate to within ±110 K [5].

As will be discussed in the following sections, it was necessary to extend the dynamic range of the temperature measurements in order to extract information below the limit of sensitivity of our color ratio pyrometry method. Since light emission scales as a power-law of temperature, we can use the pyrometry to calibrate the raw light emission signal, thus enabling us to extend the temperature measure to lower temperatures. An example of the fit between the light emission-based temperature and color-ratio pyrometry estimated temperature can be seen in Fig. 2.

2.4. Determination of transport and kinetic properties

Simultaneous determination of transport and kinetic properties in condensed reaction/diffusion systems has been of longstanding interest and a variety of methods have been developed to estimate these parameters. For a detailed discussion on these methodologies as they are related to SHS, it is recommended that the readers reference the review article by Mukasyan et al. [20]. The conversion rate ($d\eta/dt$) of an SHS reaction can be represented by superposition of a reaction kinetic term that follows Arrhenius behavior, $K(T)$, and a conversion term, $\Phi(\eta)$ (Eq. (7)) [20].

$$\frac{d\eta}{dt} = K(T)\Phi(\eta) \tag{7}$$

Previous reports by Boddington et al. suggested that the Arrhenius form of $d\eta/dt$ can be represented by Eq. (8), which consists of a pre-exponential factor (A), a conversion (η) term raised to a factor n which is representative of "nth order kinetics," and the Arrhenius exponential term where E_a is activation energy of the reaction, R is the ideal gas constant, and T is the temperature. It is important to note, however, that there are many potential kinetic rate laws which specifically apply to solid-state kinetics that could be used as an expression for $d\eta/dt$ [38]. Boddington et al. reported that other forms of $d\eta/dt$ were considered, but did not significantly change estimated values for A, n, and E_a or the quality of the fit. As such, other studies by have also used this expression to estimate kinetic parameters [37,39,40].

$$\frac{d\eta}{dt} = A(1-\eta)^n \exp\left(-\frac{E_a}{RT}\right) \tag{8}$$

Many methods have been developed to estimate E_a of SHS systems since it is fundamentally important to modeling reacting systems. One common method employed to estimate E_a involves dilution of the sample so that changes in combustion velocity are used to compute E_a [41]. However, considering that this method also inherently changes the chemistry of the reaction, an alternative proposed by Boddington et al. was favorable for the analysis presented here. Boddington et al. proposed that the conversion rate can be related to the reaction front temperature profile, thermal diffusivity, and velocity of the system by the Eq. (9) where T_{ad} is the adiabatic flame temperature, T_0 is the ambient temperature, t_r and t_d are the rise and decay times of the reaction in the remote inert regions of the reaction profile [20,36].

$$\frac{d\eta}{dt} = \frac{\frac{T-T_0}{t_d-t_r} + \frac{dT}{dt} - \frac{\alpha}{v^2}\frac{d^2T}{dt^2}}{T_{ad}-T_0} \tag{9}$$

The adiabatic flame temperature for the ZrC formation reaction (Eq. (6)) was calculated to be 3765 K using CHEETAH, though the actual temperature of the reaction would be reduced when considering side reactions with the Al [21,34,42]. Adiabatic flame temperature calculations for the 0.5 Al / 1.2 Zr / 1 C and 2 Al / 1.2 Zr / 1 C systems were estimated to be 2730 K and 1770 K, respectively, though these calculations are limited by the catalog of information available in the program for the Al-Zr-C intermediates [42]. Seeing that estimating the adiabatic flame temperature with consideration for the Al content is difficult, the adiabatic flame temperature of the ZrC formation reaction was used for calculations to estimate activation energy in the sections below. A sensitivity analysis for the role of T_{ad} on the estimated kinetic parameters revealed that changes in the adiabatic flame temperature used had a minimal impact on the activation energy.

2.5. Thermophysical property estimations

Temperature measurements collected from color-ratio pyrometry and the light emission estimates discussed in the section above were used to extract thermophysical properties of the leading and trailing edges of the reaction. Prior to any calculations, the color-ratio pyrometry temperature values were smoothed using a 2D smoothing algorithm which utilized an 8-point smoothing window [43]. Single line temperatures were extracted using a custom routine on the post-processed data that allows for data visualization at a constant vertical position.

As discussed above, light emission-based temperature estimates were used to extend the dynamic range of our temperature measurements to much lower temperatures, thus enabling us to probe the pre-reaction zone. After fitting the temperature to light intensity, the extended temperature profile was analyzed and used as inputs to the Boddington equation (Eq. (9)). Assuming that reaction at low temperatures is negligible (pre-reaction zone; i.e., $d\eta/dt = 0$), the measured combustion velocity and rise and fall time estimates from built-in MATLAB routines were used to extract values for the thermal diffusivity (α). Temperature profiles and derivative terms of the Boddington equation in the pre-reaction zone were estimated by fitting the light emission-based temperature measurements to exponential functions using built-in MATLAB fitting routines.

Thermal diffusivity of the post-reaction products was also of particular interest to examine the change in material properties after reaction. Given the gasless nature of the Al-Zr-C system, it can be assumed that heat transfer is governed exclusively by thermal conduction driven by thermal gradients [28,44]. The temperature

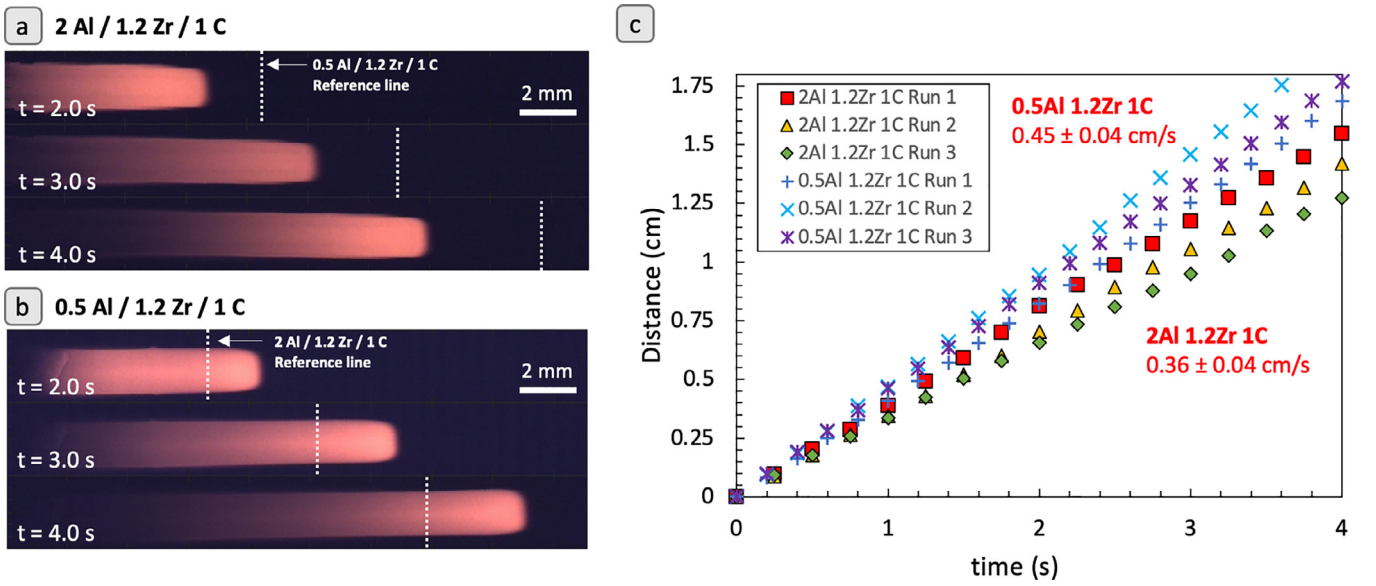

Fig. 1. (a,b) Sample high-speed images of the propagating SHS samples tested. (c) Position vs. time data for combustion of 0.5 Al / 1.2 Zr / 1 C and 2 Al / 1.2 Zr / 1 C composites in Ar measured using high speed videography. Reported velocity is based on an average of linear fits between three experiments.

of a sample as a function of position and time can therefore be roughly modeled by the heat diffusion equation (Eq. (10)) where T is temperature, x is position, and t is time. Estimations for thermal diffusivity can therefore be calculated using numerical differentiation on the pyrometry images recorded.

$$\frac{dT}{dt} = \alpha\left(\frac{d^2T}{dx^2}\right) \tag{10}$$

Initial attempts to estimate the thermal diffusivity of a sample by analyzing single point temperature as a function of time (dT/dt) and using proximity temperatures to calculate (d^2T/dt^2) numerically revealed that noise would generate unrealistic thermal diffusivities. Assuming a constant, quasi-homogeneous propagation rate, Eq. (10) can be simplified by substituting $x = vt$, where v is propagation rate (in m/s). Note that the propagation rate is shown to be very constant in Fig. 1 and that the previous work on similar stoichiometries also shows a consistent propagation rate. Thermal diffusivity can therefore be calculated using Eq. (11).

$$\frac{dT}{dx} = \frac{\alpha}{v}\left(\frac{d^2T}{dx^2}\right) \tag{11}$$

Temperature measurements used for estimating thermal diffusivity in the post reaction zone were extracted using color-ratio pyrometry values in a temperature region below the observed phase transition in the material (~1500 K). Data in this region was fit to an exponential function and those fits were then used to estimate the first and second derivatives of the thermal profile for Eq. (11).

It is also important to assess the impact of other heat losses on the surface temperature and thermal diffusivity estimations. To estimate the impact of conductive heat loss to the glass substrate, a COMSOL Multiphysics simulation of the process was performed using standard values for thermal transport properties of materials and holding a hot "reaction zone" at ~1700 K. The thermal profiles of a system with and without the glass substrate revealed that the temperature only differed by <1% and therefore we have assumed that heat loss to the substrate was negligible for the time scale over which measurements were made. Results from the COMSOL simulation can be seen in Fig. S2. A simple estimation of the relative heat fluxes due to convection and radiation also show that they play a minimal role relative to conduction in this region of interest. Both convective and radiative heat losses had an estimated flux which was <5% of that expected for conduction in the same region.

2.6. Kinetic parameter estimation

Kinetic rates were calculated using custom built routines in MATLAB using data that was extracted from the determination of the leading-edge thermal diffusivity measurements described above. By using the temperature values in the region on the leading edge above 933 K, the estimated rise and decay times, and propagation velocity, values for $d\eta/dt$ could be calculated using the Boddington equation (Eq. (9)). The values estimated by the Boddington equation and measured temperature data were then used as inputs to a MATLAB solver routine which would minimize the difference between the values calculated in Eqs. (8) and (9) to estimate values for the constants A, n, and E_a [36].

3. Results

3.1. Propagation characterization

The combustion event of samples was recorded using a high-speed camera with a resolution of ~20 μm/pixel and the leading edge of the reaction front was tracked as a function of time to calculate an average combustion velocity. Figure 1 shows position of the leading edge vs. time for the tested samples, all of which showed highly linear behavior indicating that mixing inhomogeneity from printing was not impacting the reaction velocity. Combustion velocities obtained were 0.36 ± 0.04 cm/s and 0.45 ± 0.04 cm/s for the 2 Al / 1.2 Zr / 1 C and 0.5 Al / 1.2 Zr / 1 C samples, respectively. This propagation rate is slightly lower than those reported by Vadchenko et al. (~1 cm/s), but this may be attributed to different preparation methods or heat sinks introduced by the glass substrate and polymer binder addition [35].

The inverse relationship between the Al content and combustion velocity is attributable to the change in thermal conductivity of the samples and a reduction in reaction completion as a function of Al content. A similar trend is also exhibited in work done by Arlington et al. [29,30]. The Al in the SHS system is introduced to facilitate nanolayered particle fabrication, though a side effect of the addition is an increase in the thermal conductivity of the

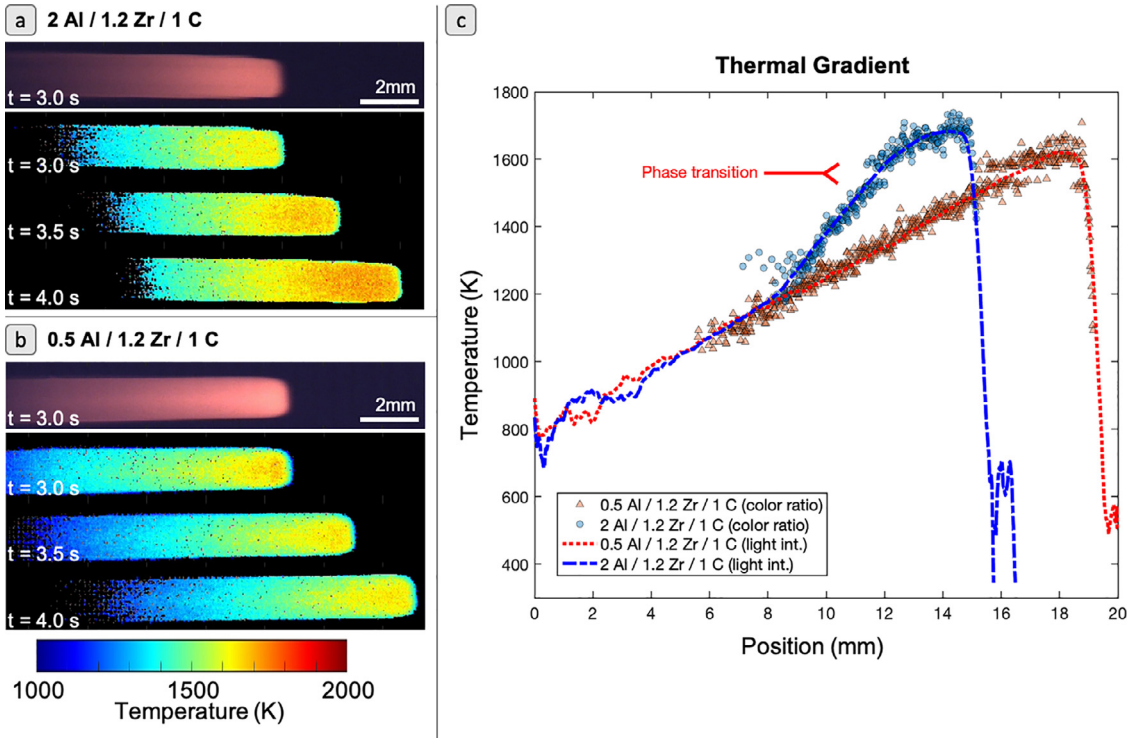

Fig. 2. (a,b) Sample color image and montage of temperature data collected via color ratio pyrometry. (c) Example of temperature vs. position data for both samples tested with regions of suspected phase transitions. Propagation direction is from left to right. Profiles shown are chosen for optimal comparison and not for the same timestamp. Dotted lines in the graph represent the light emission-based temperature measurements that are used to extend the dynamic range of the instrument.

sample. However, the Al also results in side reactions with the Zr that would decrease the overall conversion for the ZrC formation reaction. Although it has been proposed that the propagation velocity would increase with the square root of thermal diffusivity and would thereby increase with Al addition, side reactions reduce the adiabatic flame temperature for the mixture and the increased thermal diffusivity reduce the peak temperature achieved in the composite. The combined effects of the increased thermal diffusivity and reduced reaction conversion after a ~3x increase in Al content actually reduced the propagation velocity in these experiments. To further probe the role of Al content reaction dynamics, color ratio pyrometry on the propagation experiments is used in the following sections to estimate thermal profiles in-operando, thermal diffusivity of the composites, and activation energy of the reaction.

3.2. Temperature profiles

Conversion of the pixel intensities to temperature were performed using a home-built MATLAB routine that has been discussed in detail elsewhere [5]. The color ratio pyrometry code provides temperature information at each pixel location that is above the black level and not saturated. Figure 2 shows a typical thermal image via color ratio pyrometry for the propagation of the samples for a single frame without any spatial averaging. Light emission-based temperature measurements are also plotted in Fig. 2 and show a nearly perfect overlap with the color ratio temperature measurements. The accuracy in the light emission temperature measurements suggests that this correlation can be used to extend the dynamic range of our temperature measurements to estimate the rise time, decay time, and thermal diffusivity of the leading edge as will be described in the next section.

Example thermal gradients (Fig. 2) for the tested samples demonstrate two clearly different profiles. Lower Al content is associated with both wider leading and trailing edges of the thermal profile. The peak temperature of the samples is also sustained over a shorter distance for the sample with lower Al content, which is to be expected considering that the thermal conductivity of the samples should decrease with lower Al content. A similar relationship between the width of peak temperature sustainment and the Al content has also been previously reported by Hu et al. [34] The inverse relationship between the width of the trailing edge and Al content is counter to the expectation since the Al content should increase the overall thermal conductivity of the samples, though if the final product is largely a Zr/Al alloy in both samples, then these results are attributable to varied thermal properties between different alloys. A more detailed discussion is provided in the following section on thermal diffusivity. Interestingly, the peak temperature of the reaction seems to be independent of the Al content since both composites show a peak temperature ~1600–1700 K. This is counter to what would be expected as the reaction temperature was speculated to be adversely affected by side reactions of Al and Zr with increasing Al content. However, the reduction in Al content would limit the prevalence of the Zr/Al melt and the dissolution of C into the system would be inhibited, thus decreasing the degree of completion of the ZrC formation reaction, reducing the total energy release, and lowering the peak temperature.

One interesting feature of these temperature profiles is the apparent step change in temperature. This is most evident in both samples between ~1500–1600 K. We attribute this abrupt change in temperature to an endothermic phase transition, implying that there also has to be a significant increase in entropy to make the free energy thermodynamically favorable. The Al-Zr phase diagram is very rich where many equilibrium or non-equilibrium phase transitions could occur. A possible source of this endothermic phase transition is at ~1550 K from a mixture of Zr_5Al_4

Table 2
Calculated thermal diffusivities for tested SHS samples as estimated using single line temperatures and polynomial fits. Estimated kinetic parameters for tested SHS samples estimated using nonlinear regression fit and model described by Eq. (8).

Sample	Avg. Thermal Diffusivity (α), m^2/s		Kinetic Parameters		
	Leading	Trailing	A (s^{-1})	n	E_a (kJ/mol)
2 Al / 1.2 Zr / 1 C	$2.2 \pm 0.5 \times 10^{-6}$	$7.2 \pm 2.2 \times 10^{-5}$	122 ± 60	2.3 ± 0.8	31 ± 4
0.5 Al / 1.2 Zr / 1 C	$2.6 \pm 0.1 \times 10^{-6}$	$1.1 \pm 0.1 \times 10^{-4}$	184 ± 79	2.6 ± 0.5	34 ± 4

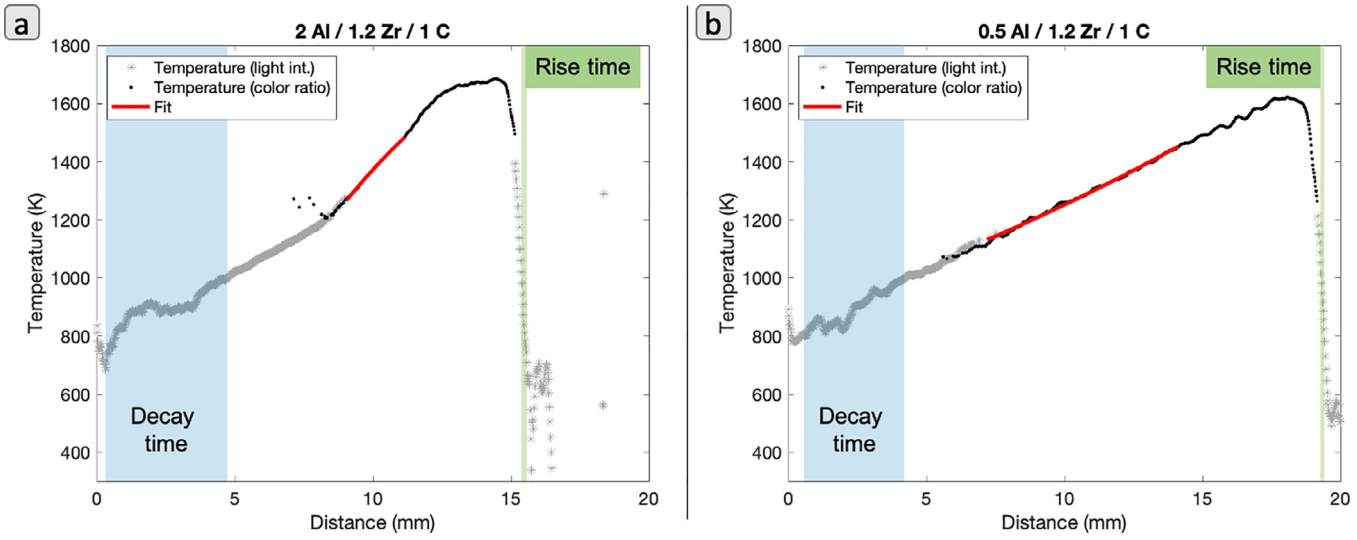

Fig. 3. Temperature profile data for (a) 2 Al / 1.2 Zr / 1C and (b) 0.5 Al / 1.2 Zr / 1 C printed samples. Solid line in each plot shows the goodness of fit for the exponential curve used to estimate thermal diffusivity on trailing edge. Shaded regions highlight the regions used for rise and decay time where temperature is <933 K.

($\Delta H_f = -0.4$ eV/atom) and Zr_2Al_3 ($\Delta H_f = -0.5$ eV/atom) to a mixture of ZrAl ($\Delta H_f = -0.27$ eV/atom) and Zr_2Al_3 [45].

There was also a phenomenon observed in both samples where the light intensity would cyclically spike during sample propagation, though this was most prominent in the 2 Al / 1.2 Zr / 1 C case. A plot of light intensity vs. time for the 2 Al / 1.2 Zr / 1 C (Fig. S3) exhibits periodic oscillations occurring at a frequency of 1 Hz (1 cycle/s, ~0.36 cm/cycle) with temperature oscillations of ~50–100 K. One possible cause of the oscillations is that the sample is propagating in a "relay-race mode" where there are local hesitations in the reaction front because of thermal resistances between distinctly separated reaction regions [18,26,27,44]. However, it is unlikely that the sample is propagating in relay-race mode since the oscillations are periodic and that the length scale of the reaction front (~1–2 mm, Fig. 2c) is roughly 2–3 orders of magnitude larger than that of the composite powders (Fig. S1) [26–28,44,46–48]. Videos recorded of the flame front with enhanced magnification (Fig. S4) also show no evidence of resolved flame corrugation, casting further doubt on the notion of relay-race mode propagation. All of these observations, in addition to the linearity of the velocity profiles, suggest that this SHS system is within the quasi-homogenous propagation regime [44]. Such auto-oscillations have been reported in a variety of SHS systems and are widely agreed to originate from unsteady heat transfer in the reacting medium, whether it be driven by limitations in heat and mass transfer rates or multi-step reactions in SHS [19,49–53]. Unlike many of the studies that seek to numerically evaluate the oscillations in these materials, we do not see any hesitations in the propagation velocity. Overall, the origins of these oscillations are complex and not entirely understood [54]. The observation is noted here for thoroughness but is not considered further.

3.3. Extraction of thermophysical properties

Thermophysical properties were extracted using a mixture of methods with data from the color ratio pyrometry and light emission-based temperature measurements. The resulting thermal diffusivity data has been summarized in Table 2. Example plots of the temperature data in the different regions, polynomial fits for the trailing edge estimation, and regions used for the rise and decay regions can be seen in Fig. 3.

As discussed in the experimental section, the light emission temperature measurements were used as inputs for the Boddington equation. At temperatures below 933 K, it can be reasonably assumed that there is negligible chemistry and therefore the left-hand side of the Boddington equation can be set to 0. Built-in MATLAB routines to identify the rise and decay times of the SHS reaction, temperature measurements, and combustion velocity were used to estimate thermal diffusivity. For the leading edge of the samples, the thermal diffusivity was nominally ~2×10^{-6} m^2/s between both samples. Although these thermal diffusivity values are relatively low, the numerous interfaces between the ~µm sized particles and different materials within the particles would lower the thermal conductivity of the sample and therefore these values are believed to be reasonable.

On the trailing edge of the sample, the thermal diffusivity increased by ~30–40x for both samples. This increase in thermal diffusivity on the trailing edge is the primary goal of Draper's RAIL3D program to create printable, reactive materials that have a higher conductivity after reaction [29,31]. This diffusivity enhancement suggests that the reaction is mostly complete before the temperature begins decreasing. The high temperatures reached during the reaction also results in particle melting and sintering which promotes conductivity/diffusivity. This result is also consistent with

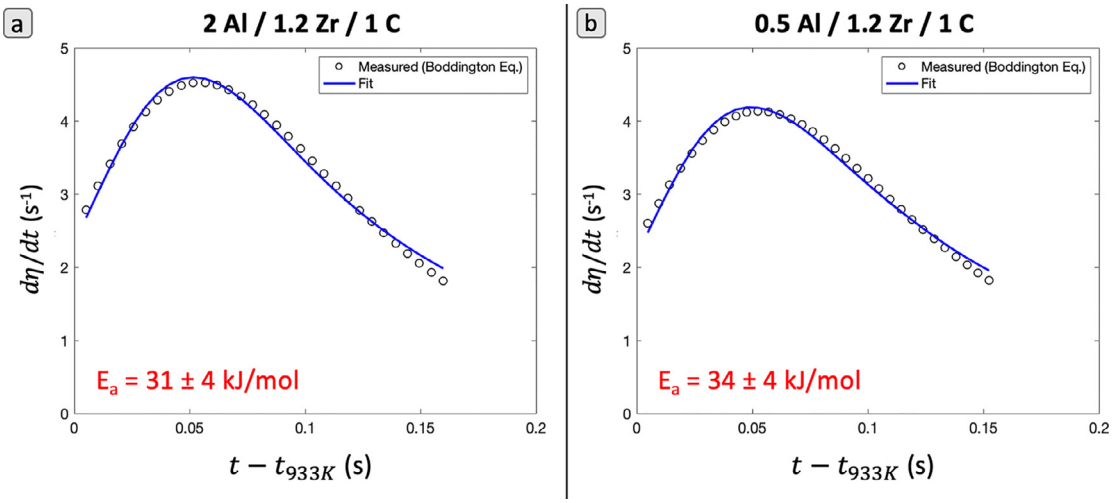

Fig. 4. Plots of dη/dt vs. time and corresponding Arrhenius model fit used to calculate the activation energy of (a) 2 Al / 1.2 Zr / 1 C and (b) 0.5 Al / 1.2 Zr / 1 C samples. Timestamps were normalized to time after the reaction front profile exceeded 933 K.

those reported in Arlington et al. [29] Interestingly, samples with higher Al content had a lower thermal diffusivity, which may seem counterintuitive since the final products are ideally Al and ZrC Eqs. (2)–((6)) and Al is a very good thermal conductor. This behavior is likely traceable to the role of Al as a diluent in the reaction, thus larger amounts of Al could detract from the energy output of the reaction, reduce the ability for Al to reflow heat, and lead to incomplete reactions which has products/morphologies with lower thermal diffusivity [29,34]. The depression in the measured thermal diffusivity compared to the values of the pure components can be largely attributed to the introduction of a polymer binder for the printing process, interfacial resistances between the powder grains, and porosity in the materials. For reference, the thermal diffusivities of Al, Zr, and C are roughly 9.7 × 10^{-5} m^2/s, 1.2 × 10^{-5}, and 2.2 × 10^{-4} m^2/s, respectively.

3.4. Kinetic parameters

Arrhenius parameters and reaction order in Eq. (8) were determined using a nonlinear regression fit of Eq. (8) to the experimentally-determined $d\eta/dt$. Activation energies reported have been calculated for temperatures on the leading edge of the thermal profile (T>933 K). A summary of the kinetic parameters use as inputs for Eq. (8) can be seen in Table 2.

Plots of $d\eta/dt$ versus time and corresponding Arrhenius model fits of the two mixtures are presented in Fig. 4. Plots of η versus time corresponding to the data presented in Fig. 4 can be seen in Fig. S5. The Arrhenius model fits are in good agreement with the measured data for $d\eta/dt$. Pre-exponential factors (A) were ~122 ± 60 s^{-1} and ~184 ± 79 s^{-1} for the 2 Al / 1.2 Zr / 1 C and 0.5 Al / 1.2 Zr / 1 C curve fits, respectively. The reaction order(s) (n) in the curve fits were nominally between 2.3–2.6, which is representative of a complex, multistep reaction mechanism proposed for the system [21,32–34]. Activation energies for the 2 Al / 1.2 Zr / 1 C and 0.5 Al / 1.2 Zr / 1 C composites were estimated to be ~31 ± 4 kJ/mol and ~34 ± 4 kJ/mol, respectively. These activation energies are lower than values that were previously reported for similar Al-Zr-C composites when estimated using differential thermal analysis (99–186 kJ/mol) [20,34]. We note, however, that Boddington et al. also reported lower activation energies which they attributed to discrepancies in experimental conditions [36]. In particular, they suggested that kinetic analysis under ignition conditions will yield a different apparent activation energy than that obtained under steady reaction propagation as was done in this work. This is not particularly surprising as they are very different processes and similar behavior has been reported for gas phase combustion. Therefore, the activation energy measured here represents the thermal sensitivity of the mass burning rate, which is a convolution of the thermal sensitivity to heat/mass transfer and the chemistry.

The slight change in the estimated activation energies for the different composites is likely not significant, although it has been previously reported that an increase in Al would promote the Al-Zr intermetallic reaction which has a lower activation energy than the ZrC formation reaction [34]. Again, these values are meant to be representative of the bulk material under experimental conditions which could be used as inputs to a thermal propagation model.

4. Conclusion

This work investigates the propagation and thermophysical properties of an additively manufactured, self-propagating high-temperature synthesis (SHS) Al-Zr-C composite. By employing high-speed color ratio pyrometry, the temperature profile of the SHS compound was measured in-operando for two samples with varied stoichiometry. High-speed videography and pyrometry analysis of the reaction event showed that propagation velocity of the samples was 0.3–0.5 cm/s and varied inversely with Al content. These propagation events also demonstrated auto-oscillations in reactions associated with temperature rises of ~50–100 K at a frequency of 1 Hz. Using the temperature measurements, the thermal diffusivity of the samples was estimated using the thermal diffusion equation to be ~2 × 10^{-6} m^2/s on the leading edge of the reaction front and both samples exhibited a >30x increase in thermal diffusivity on the trailing edge. The increase in thermal diffusivity exhibited the desired behavior to have a material undergo a reaction which results in a conductivity enhancement over the starting material. Activation energy of the two samples was estimated to be ~30–35 kJ/mol. This work ultimately demonstrates a new, accessible measurement methodology that could be used to estimate thermophysical changes in materials for generalized modeling purposes.

Declaration of Competing Interest

The authors have no financial interests.

Acknowledgments

The authors would like to acknowledge the Charles Stark Draper Laboratory (CSDL) for providing materials for this study. This work was funded by the Air Force Office of Scientific Research and the Army Research Office.

Supplementary materials

Supplementary material associated with this article can be found, in the online version, at doi:10.1016/j.combustflame.2020.12.045.

References

[1] A.M. Golobic, M.D. Durban, S.E. Fisher, M.D. Grapes, J.M. Ortega, C.M. Spadaccini, E.B. Duoss, A.E. Gash, K.T. Sullivan, Active mixing of reactive materials for 3D printing, Adv. Eng. Mater. 21 (2019) 1900147, doi:10.1002/adem.201900147.
[2] H. Wang, D.J. Kline, M. Rehwoldt, T. Wu, W. Zhao, X. Wang, M.R. Zachariah, Architecture can significantly alter the energy release rate from nanocomposite energetics, ACS Appl. Polym. Mater. 1 (2019) 982–989, doi:10.1021/acsapm.9b00016.
[3] L.J. Groven, M.J. Mezger, Printed Energetics: The Path Toward Additive Manufacturing of Munitions, CRC Press (2017), pp. 115–128.
[4] H. Wang, J. Shen, D.J. Kline, N. Eckman, N.R. Agrawal, T. Wu, P. Wang, M.R. Zachariah, Direct writing of a 90 wt% particle loading nanothermite, Adv. Mater. 31 (2019) 1806575, doi:10.1002/adma.201806575.
[5] R.J. Jacob, D.J. Kline, M.R. Zachariah, High speed 2-dimensional temperature measurements of nanothermite composites: probing thermal vs. gas generation effects, J. Appl. Phys. 123 (2018) 115902, doi:10.1063/1.5021890.
[6] H. Wang, D.J. Kline, M.R. Zachariah, In-operando high-speed microscopy and thermometry of reaction propagation and sintering in a nanocomposite, Nat. Commun. 10 (2019) 3032, doi:10.1038/s41467-019-10843-4.
[7] W.P. Bassett, D.D. Dlott, Multichannel emission spectrometer for high dynamic range optical pyrometry of shock-driven materials, Rev. Sci. Instrum. 87 (2016), doi:10.1063/1.4964386.
[8] W. Zhao, X. Wang, H. Wang, T. Wu, D.J. Kline, M. Rehwoldt, H. Ren, M.R. Zachariah, S. Holdren, M. Rehwoldt, H. Ren, M.R. Zachariah, Titanium enhanced ignition and combustion of Al/I2O5 mesoparticle composites, Combust. Flame 212 (2020) 245–251, doi:10.1016/j.combustflame.2019.04.049.
[9] M.C. Rehwoldt, H. Wang, D.J. Kline, T. Wu, N. Eckman, P. Wang, N.R. Agrawal, M.R. Zachariah, Ignition and combustion analysis of direct write fabricated aluminum/metal oxide/PVDF films, Combust. Flame 211 (2020) 260–269, doi:10.1016/j.combustflame.2019.08.023.
[10] K.T. Sullivan, C. Zhu, E.B. Duoss, A.E. Gash, D.B. Kolesky, J.D. Kuntz, J.A. Lewis, C.M. Spadaccini, Controlling material reactivity using architecture, Adv. Mater. 28 (2016) 1934–1939, doi:10.1002/adma.201504286.
[11] D.K. Smith, D.K. Unruh, C.C. Wu, M.L. Pantoya, Replacing the Al2O3 shell on Al particles with an oxidizing salt, aluminum iodate hexahydrate. Part I: reactivity, J. Phys. Chem. C 121 (2017) 23184–23191, doi:10.1021/acs.jpcc.7b05803.
[12] D.J. Kline, M.C. Rehwoldt, C.J. Turner, P. Biswas, G.W. Mulholland, S.M. McDonnell, M.R. Zachariah, Spatially focused microwave ignition of metallized energetic materials, J. Appl. Phys. 127 (2020) 55901, doi:10.1063/1.5134089.
[13] R.J. Jacob, K.J. Hill, Y. Yang, M.L. Pantoya, M.R. Zachariah, Pre-stressing aluminum nanoparticles as a strategy to enhance reactivity of nanothermite composites, Combust. Flame 205 (2019) 33–40, doi:10.1016/j.combustflame.2019.03.024.
[14] D.J. Kline, M.C. Rehwoldt, H. Wang, N.E. Eckman, M.R. Zachariah, Why does adding a poor thermal conductor increase propagation rate in solid propellants? Appl. Phys. Lett. 115 (2019) 114101, doi:10.1063/1.5113612.
[15] H. Wang, J.B. DeLisio, S. Holdren, T. Wu, Y. Yang, J. Hu, M.R. Zachariah, Mesoporous silica spheres incorporated aluminum/poly (vinylidene fluoride) for enhanced burning propellants, Adv. Eng. Mater. 20 (2018) 1–7, doi:10.1002/adem.201700547.
[16] J. Shen, H. Wang, D.J. Kline, Y. Yang, X. Wang, M. Rehwoldt, T. Wu, S. Holdren, M.R. Zachariah, Combustion of 3D printed 90 wt% loading reinforced nanothermite, Combust. Flame 215 (2020) 86–92, doi:10.1016/j.combustflame.2020.01.021.
[17] S. Isert, C.D. Lane, I.E. Gunduz, S.F. Son, Tailoring burning rates using reactive wires in composite solid rocket propellants, Proc. Combust. Inst. 36 (2017) 2283–2290, doi:10.1016/j.proci.2016.06.141.
[18] A. Varma, A.S. Rogachev, A.S. Mukasyan, S. Hwang, Complex behavior of self-propagating reaction waves in heterogeneous media, Proc. Natl. Acad. Sci. U.S.A. 95 (1998) 11053–11058, doi:10.1073/pnas.95.19.11053.
[19] I.P. Borovinskaya, A. Gromov, E.A. Levashov, Y.M. Maksimov, A.S. Mukasyan, A.S. Rogachev, Concise Encyclopedia of Self-Propagating High-Temperature Synthesis : History, Theory, Technology, and Products, Elsevier, 2017.
[20] A.S. Mukasyan, C.E. Shuck, Kinetics of SHS reactions: a review, Int. J. Self Propag. High Temp. Synth. 26 (2017) 145–165, doi:10.3103/S1061386217030049.
[21] M.S. Song, M.W. Ran, Y.Y. Kong, In situ fabrication of ZrC powder obtained by self-propagating high-temperature synthesis from Al-Zr-C elemental powders, Int. J. Refract. Met. Hard Mater. 29 (2011) 392–396, doi:10.1016/j.ijrmhm.2011.01.013.
[22] A.S. Mukasyan, A.S. Rogachev, M. Mercedes, A. Varma, Microstructural correlations between reaction medium and combustion wave propagation in heterogeneous systems, Chem. Eng. Sci. 59 (2004) 5099–5105, doi:10.1016/j.ces.2004.07.043.
[23] A.S. Mukasyan, A.S. Rogachev, A. Varma, Mechanisms of reaction wave propagation during combustion synthesis of advanced materials, Chem. Eng. Sci. 54 (1999) 3357–3367, doi:10.1016/S0009-2509(98)00457-6.
[24] S. Vummidi Lakshman, J.D. Gibbins, E.R. Wainwright, T.P. Weihs, The effect of chemical composition and milling conditions on composite microstructure and ignition thresholds of Al–Zr ball milled powders, Powder Technol. 343 (2019) 87–94, doi:10.1016/j.powtec.2018.11.012.
[25] M. Schoenitz, T.S. Ward, E.L. Dreizin, Fully dense nano-composite energetic powders prepared by arrested reactive milling, Proc. Combust. Inst. 30 (2005) 2071–2078, doi:10.1016/j.proci.2004.08.134.
[26] S. Hwang, A.S. Mukasyan, A. Varma, Mechanisms of combustion wave propagation in heterogeneous reaction systems, Combust. Flame 115 (1998) 354–363, doi:10.1016/S0010-2180(98)00016-9.
[27] A.G. Merzhanov, A.S. Mukas'yan, A.S. Rogachev, A.E. Sychev, S. Hwang, A. Varma, Combustion-front microstructure in heterogenous gasless media, Combust. Explos. Shock Waves. 32 (1996) 655–666.
[28] F.D. Tang, A.J. Higgins, S. Goroshin, Effect of discreteness on heterogeneous flames: propagation limits in regular and random particle arrays, Combust. Theory Model. 13 (2009) 319–341, doi:10.1080/13647830802632184.
[29] S.Q. Arlington, S. Vummidi Lakshman, S.C. Barron, J.B. DeLisio, J.C. Rodriguez, S. Narayanan, G.M. Fritz, T.P. Weihs, Exploring material chemistry for direct ink writing of reactively formed conductors, Mater. Adv. 1 (2020) 1151–1160, doi:10.1039/d0ma00148a.
[30] S.Q. Arlington, S.C. Barron, J.B. DeLisio, J.C. Rodriguez, S.V. Lakshman, T.P. Weihs, G.M. Fritz, Multifunctional reactive nanocomposites via direct ink writing, (2020).
[31] G.M. Fritz, S. Barron, Reactively assisted ink for printed electronic circuits, (2019).
[32] M. Song, B. Huang, M. Zhang, J. Li, Reaction synthesis of nano-scale ZrC particulates by self-propagating high-temperature synthesis from Al-Zr-C powder mixtures, ISIJ Int. 48 (2008) 1026–1029, doi:10.2355/isijinternational.48.1026.
[33] M.S. Song, B. Huang, M.X. Zhang, J.G. Li, In situ synthesis of ZrC particles and its formation mechanism by self-propagating reaction from Al-Zr-C elemental powders, Powder Technol. 191 (2009) 34–38, doi:10.1016/j.powtec.2008.09.005.
[34] Q. Hu, M. Zhang, P. Luo, M. Song, J. Li, Thermal explosion synthesis of ZrC particles and their mechanism of formation from Al-Zr-C elemental powders, Int. J. Refract. Met. Hard Mater. 35 (2012) 251–256, doi:10.1016/j.ijrmhm.2012.06.008.
[35] S.G. Vadchenko, D.Y. Kovalev, M.A. Luginina, Ignition and phase formation in the Zr–Al–C system, Combust. Explos. Shock Waves 53 (2017) 171–175, doi:10.1134/S0010508217020071.
[36] T. Boddington, P.G. Laye, J. Tipping, D. Whalley, Kinetic analysis of temperature profiles of pyrotechnic systems, Combust. Flame 63 (1986) 359–368, doi:10.1016/0010-2180(86)90005-2.
[37] S.D. Dunmead, Z.A. Munir, J.B. Holt, Temperature profile analysis in combustion synthesis: II, experimental observations, J. Am. Ceram. Soc. 75 (1992) 180–188, doi:10.1111/j.1151-2916.1992.tb05462.x.
[38] A. Khawam, D.R. Flanagan, Solid-state kinetic models: basics and mathematical fundamentals, J. Phys. Chem. B 110 (2006) 17315–17328, doi:10.1021/jp062746a.
[39] F. Baras, Determination of transport and kinetic properties in self-propagating high-temperature synthesis, J. Alloys Compd. 455 (2008) 113–120, doi:10.1016/j.jallcom.2007.01.076.
[40] M. Marinšek, J. Kemperl, B. Likozar, J. Maček, Temperature profile analysis of the citrate-nitrate combustion system, Ind. Eng. Chem. Res. 47 (2008) 4379–4386, doi:10.1021/ie800296m.
[41] A.G. Merzhanov, New elementary combustion models of 2nd kind, Dokl. Akad. Nauk SSSR 233 (1977) 1130–1133.
[42] S. Bastea, L.E. Fried, K.R. Glaesemann, W.M. Howard, P.C. Sovers, P.A. Vitello, CHEETAH 5.0, User's Manual, Lawrence Livermore Natl. Lab, Livermore, CA., 2006.
[43] G. Reeves, Smooth2a, (2009).
[44] A. Varma, A.S. Mukasyan, S. Hwang, Dynamics of self-propagating reactions in heterogeneous media: experiments and model, Chem. Eng. Sci. 56 (2001) 1459–1466, doi:10.1016/S0009-2509(00)00371-7.
[45] M. Alatalo, M. Weinert, R.E. Watson, Stability of Zr-Al alloys, Phys. Rev. B 57 (1998) R2009.
[46] J.M. Beck, V.A. Volpert, Nonlinear dynamics in a simple model of solid flame microstructure, Phys. D Nonlinear Phenom. 182 (2003) 86–102, doi:10.1016/S0167-2789(03)00119-2.
[47] A.S. Rogachev, Microheterogeneous mechanism of gasless combustion, Combust. Explos. Shock Waves 39 (2003) 150–158, doi:10.1023/A:1022956915794.
[48] A.S. Rogachev, F. Baras, Models of SHS: an overview, Int. J. Self Propag. High Temp. Synth. 16 (2007) 141–153, doi:10.3103/s1061386207030077.
[49] J.Y. Zhang, Z.Y. Fu, W.M. Wang, Q.J. Zhang, Theoretical study on auto-oscillating combustion in self-propagating high temperature synthesis, J. Wuhan Univ. Technol. Mater. Sci. Ed. 18 (2003) 32–34, doi:10.1007/bf02838385.

[50] K.G. Shkadinskii, B.I. Khaikin, A.G. Merzhanov, Propagation of a pulsating exothermic reaction front in the condensed phase, Combust. Explos. Shock Waves 7 (1971) 15–22.
[51] M.G. Lakshmikantha, J.A. Sekhar, An investigation of the effect of porosity and diluents on micropyretic synthesis, Metall. Trans. A 24 (1993) 617–628, doi:10.1007/BF02656631.
[52] A. Bayliss, A. Bayliss, B.J. Matkowsky, B.J. Matkowsky, Two routes to chaos in condensed phase combustion, SIAM J. Appl. Math. 50 (1990) 437–459, doi:10.1137/0150026.
[53] A.S. Mukasyan, A.S. Rogachev, A. Varma, Mechanisms of pulsating combustion during synthesis of advanced materials, AIChE J. 45 (1999) 2580–2585, doi:10.1002/aic.690451214.
[54] K.G. Shkadinsky, A.S. Rogachev, Auto-oscillations, in: I.P. Borovinskaya, A.A. Gromov, E.A. Levashov, Y.M. Maksimov, A.S. Mukasyan (Eds.), A.S.B.T.-C.E. of S.-P.H.-T.S. Rogachev, Eds., Elsevier, Amsterdam (2017), pp. 22–23, doi:10.1016/B978-0-12-804173-4.00010-7.